An Available Method Utilizing the Waste Heat in a Direct Carbon Fuel Cell

Liwei Chen[1], Houcheng Zhang[2,*], Songhua Gao[1]

[1]School of Mechanical & Electronic Engineering, Sanming University, Sanming 365004, China;
[2]Department of Microelectronic Science and Engineering, Ningbo University, Ningbo 315211, China
*E-mail: zhanghoucheng@nbu.edu.cn

A new hybrid system is established to utilize the waste heat generated in a DCFC (direct carbon fuel cell). The hybrid system mainly consists of a DCFC with molten carbonate as electrolyte, a regenerator and a Carnot heat engine, where the Carnot heat engine is driven by the high-quality waste heat generated in the DCFC. Based on the electrochemistry and non-equilibrium thermodynamics, expressions for the efficiencies and power outputs of the DCFC, Carnot heat engine and hybrid system are derived, where the different sources of irreversible losses such as the various kinds of overpotentials in the electrochemical reaction process, finite-rate heat transfer between the DCFC and the heat engine, and heat-leak from the DCFC to the environment are considered. It shows that the performance of the DCFC can be greatly enhanced by coupling a Carnot heat engine to further convert the waste heat for power generation. By employing numerical calculations, the effects of some design parameters and operating conditions on the performance of the hybrid system are discussed in detail. The investigation method in the present paper is feasible for some other similar energy conversion systems as well.

1. INTRODUCTION

Fuel cells have been heralded as a replacement for current less efficient power generation technologies because of their high efficiency and zero toxic emission levels. The applications of fuel cells are enormous and include large scale stationary power generation, distributed combined heat and power and portable power [1-3]. Among all possible fuels for fuel cells, hydrogen is the preferred

choice as high power density for fuel cells can be achieved. However, effective and economic production and storage as well as refueling infrastructure are still facing with big challengers.

Compared with the prevailing hydrogen fuel, carbon is more convenient for storage and transportation and is less fire/explosion hazard. DCFC (direct carbon fuel cell) is a unique electrochemical device which can directly converts the chemical energy of carbon or biomass into electricity without the need for gasification or the moving machinery associated with conventional electric generators [4-6]. Almost all the carbon-rich materials such as coal, natural gas, petroleum, and biomass can be easily converted or purified to the fuel of DCFC. Thus, the DCFC is considered as one of the most attractive solution in the automotive and power generation industry [6-10].

Generally, the working temperature range of DCFC is 973~1073 K [6, 9, 10], and there will be a lot of high-quality waste heat production when the DCFC is put into operation. Thus, it is a task deserving deeply investigation on how to availably utilize the waste heat produced in DCFC. The high-temperature operating characteristics provide the possibility of cogeneration with other types of power generators such as gas turbines or heat engines for further power generation. So far, numerous investigators have carried out on the high-temperature fuel cells such as the solid oxide fuel cells (SOFCs) and molten carbonate fuel cells (MCFCs) based hybrid systems in order to increase the overall performance of the fuel cells [11-15], however, the study on further utilizing the waste heat in DCFCs for power generation through heat engine hybrid system is seldom, the existing method for improving the efficiency for DCFC is always considered a hybrid electrode configuration [16].

In the present paper, we will construct a new typical system to effectively recover the waste heat generated in the DCFC for power generation, the hybrid system mainly composed of a DCFC, a regenerator and a Carnot heat engine. Each component in the hybrid system will be dividedly described, and the numerical expressions for efficiency and power output of the hybrid system are derived by considering not only the irreversible losses in the DCFC but also the heat-leak from the fuel cell to the environment as well as the heat transfer between the fuel cell and the heat engine. Based on numerical calculations, the general performance characteristics are revealed and the optimal regions for some important performance parameters are given, and consequently, the performance characteristics of the hybrid system are optimized.

2. AN IRREVERSIBLE MODEL OF THE DCFC-CARNOT HEAT ENGINE HYBRID SYSTEM
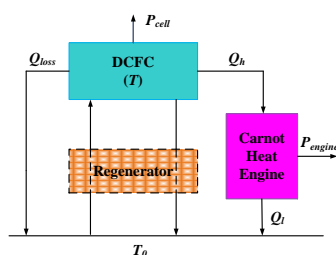

Figure 1. The schematic diagram of an irreversible DCFC-Carnot heat engine hybrid system.

Figure 1 shows the schematic diagram of a DCFC-Carnot heat engine hybrid system, which mainly consists of a DCFC, a Carnot heat engine and a regenerator. The DCFC in the hybrid system plays a role of the high-temperature heat reservoir of the Carnot engine which is employed for a further power generation. The regenerator acts as a counter-flow heat exchanger, which economically absorbs the heat in the high-temperature exhaust gas to preheat the reactants to attain the reaction temperature.

In order to quantitatively analyze the performance of the whole hybrid system, the following major assumptions are often adopted [15, 17-20]:

(1)   Both the DCFC and the Carnot engine are operated under steady-state condition;

(2)   The regenerator is regarded as a perfect one;

(3)   Operating temperature and pressure are uniform and constant in the DCFC;

(4)   All gases involved are assumed to be compressible ideal gases;

(5)   The carbon fuel is regarded as a rigid sphere and packed with a simple hexagonal pattern;

(6)   The concentration overpotential in the anode is assumed to be negligible.

In the following, we will individually analyze each component in the hybrid system and then globally study the performance of the whole hybrid system.
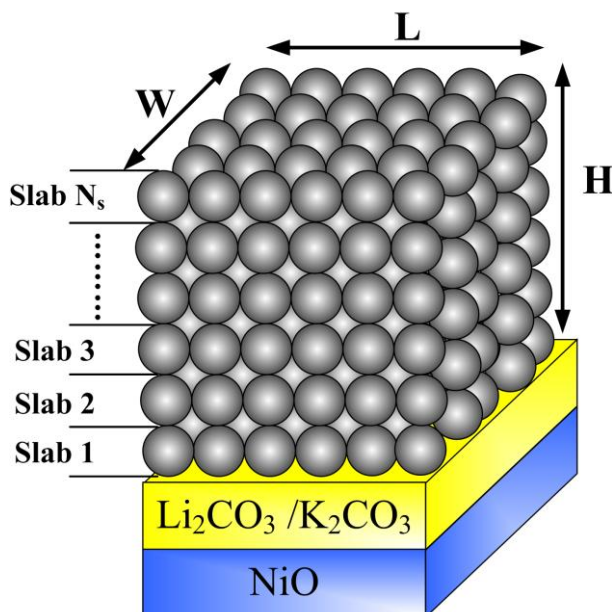
2.1. The DCFC

Figure 2. The schematic diagram of a packed bed anode DCFC with molten carbonate electrolyte.

The DCFC model presented in this study has been previously reported in Ref. [20]. As shown in Figure 2, the DCFC consists of a packed bed anode, a porous cathode, and a molten carbonate

electrolyte sandwiched in between the two electrodes, where the anode, electrolyte, and cathode are made of graphite, Li_2CO_3/K_2CO_3 eutectic melt with a molar ratio of 32:68, and lithium doped NiO, respectively [7, 20]. DCFC converts the chemical energy in a carbon fuel directly into electricity without the need for gasification. Fine (submicron) carbon particles in an electrochemical cell are electrochemically oxidized at high temperature with the overall fuel cell reaction being: $C + O_2 \rightarrow CO_2$. The reactions in DCFC produce almost pure CO_2 [21-25], the provided high purity graphite can be contained in a concentrated stream and easily captured for downstream use or disposal avoiding the need for costly gas separation technologies. The basic thermodynamic relationship for the overall reaction in the DCFC can be given as [7, 8, 20]

$$-\Delta \overset{\cdot}{H} = -\frac{\Delta h}{n_e F} I \,, \tag{1}$$

where n_e is the number of mole electrons transferred per mole graphite ($n_e = 4$), F is Faraday's constant, I is the operating electric current of the DCFC [19], and $(-\Delta h)$ is the molar enthalpy change which can be calculated from the data provide in Ref. [20]. According to the basic thermodynamic relationship: $-\Delta H = -\Delta G - T\Delta S$, the total energy $(-\Delta H)$ can be divided into two parts, i.e., $(-\Delta G)$ and $(-T\Delta S)$, which are representative of electrical energy and thermal energy, respectively. As long as the enthalpy change is more negative than the Gibbs free energy change of the reaction, the part of the total energy, $(-T\Delta S)$, cannot be converted to electrical energy, which will be released as heat [14, 15].

Based on the model established by Zhang et al. [20], the power output and efficiency of the DCFC can be, respectively, expressed as

$$P_{cell} = JA\left(E - V_{act,\text{an}} - V_{act,\text{cat}} - V_{ohm} - V_{con}\right), \tag{2}$$

and

$$\eta_{cell} = \frac{P}{-\Delta \overset{\cdot}{H}}$$
$$= -\frac{n_e F}{\Delta h}\left(E - V_{act,\text{an}} - V_{act,\text{cat}} - V_{ohm} - V_{con}\right), \tag{3}$$

where

$$E = -\frac{\Delta g^0(T)}{n_e F} + \frac{RT}{n_e F}\ln\left[\frac{p_{O_2,\text{cat}}\left(p_{CO_2,\text{cat}}\right)^2}{p_{CO_2,\text{an}}}\right], \tag{4}$$

$$V_{act,\text{an}} = \frac{RT}{2F}\ln\left[\frac{J}{2K_B\exp\left(-E_B/T\right)} + \sqrt{\left(\frac{J}{2K_B\exp\left(-E_B/T\right)}\right)^2 + 1}\right], \tag{5}$$

$$V_{act,\text{cat}} = \frac{RT}{2F}\ln\left[\frac{J}{2J^0_{0,cat}(p_{CO_2,\text{cat}})^{r_1}(p_{O_2,\text{cat}})^{r_2}} + \sqrt{\left(\frac{J}{2J^0_{0,cat}(p_{CO_2,\text{cat}})^{r_1}(p_{O_2,\text{cat}})^{r_2}}\right)^2 + 1}\right], \tag{6}$$

$$V_{ohm} = \sum_{i=1}^{N_s} J \frac{D_c}{\sigma_s^0 \varepsilon^{1.5} \exp(-E_a/RT)} \left[1 - \frac{N_e}{LW} \sqrt{\frac{(N_s-i)F_g - F_r}{\pi cM}} \right] + \sum_{i=1}^{N_s} JN_e \frac{\sqrt{3}D_c^2}{4LW\sigma_{c,0}}$$

$$+ J \left[\frac{A}{p_{O_2,cat}^{0.67}} \exp(B/T) + C_R + D\exp(f/T) \right], \qquad (7)$$

$$V_{con} = \frac{RT}{n_e F} \ln \left(\frac{J_{lim}}{J_{lim} - J} \right), \qquad (8)$$

J is the operating current density; the subscripts "an" and "cat" indicate, respectively, "anode" and "cathode"; the p_k are the partial pressures of species k at the anode or cathode; $\Delta g^0(T)$ is the Gibbs free energy change at the standard pressure (1 atm) which can be calculated from the data in Ref. [20] ; N_s is the number of the slabs, which depends on the bed height H and the diameter of the carbon particle D_c, i.e., $N_s = H/D_c$; F_g is the vertical gravitational force of an graphite particle; F_r is the repulsive force between two neighboring particles; ε is the voidage of the packed bed; $\sigma_{c,0}$ is the conductivity of the graphite particle; M is the stress at the elastic limit, c is related to the shape and size of the surface irregularities; $J_{lim} = n_e F K_{CO_2} C_{CO_2}^b$ is the limiting current density, K_{CO_2} is the mass transportation coefficient of CO_2, and $C_{CO_2}^b$ is the concentration of CO_2 in the bulk; and the values of parameters used in the modeling of DCFC are listed in Table 1 [7, 20, 26].

Table 1. Parameters used in the modeling of a DCFC [7, 20, 26].

Parameter	Value
Charge transfer coefficient, β	0.5
Operating pressure, P (Pa)	1.01325×10^5
Ideal gas constant, R (J/mol K)	8.314
Faraday constant, F (C/mol)	96,485
Height of packed bed anode, H (m)	1.0×10^{-3}
Length of packed bed anode, L (m)	1.0×10^{-2}
Width of packed bed anode, W (m)	1.0×10^{-2}
Diameter of spherical graphite particle, D_c (m)	1.0×10^{-5}
Concentration independent cathode exchange current density, $j_{0,cat}^0$ (A/m^2)	5.0×10^2
Conductivity of electrode phase, $\sigma_{c,0}$ (s/m^2)	1.6×10^5
Density of graphite particle, ρ_c (kg/m^3)	1.5×10^3
Density of electrolyte, ρ_e (kg/m^3)	2.0×10^3
Acceleration of gravity, g (m/s^2)	9.8
Pre-exponential factor of the backward reaction, K_B (A/m^2)	5.8×10^9
Temperature activation of the backward reaction, E_B (K^{-1})	22,175
exponential factor for Eq. (7), σ_s^0 (s/m^2)	2.322×10^5

Apparent activation energy in Eq. (7), E_a (J/mol)	2.191×10^4
Mass transport coefficient of CO_2, K_{CO_2} (m/s)	3.5×10^{-2}
Constant in Eq. (6), r_1	-1.250
Constant in Eq. (6), r_2	0.375
Bulk gas compositions at the cathode side	67%CO_2/33% O_2
Operating temperature of DCFC, T (K)	923
Temperature of environment, T_0 (K)	298

2.2. The Carnot heat engine

Figure 3. The schematic diagram of an endoreversible Carnot heat engine.

For the sake of convenience, an endoreversible Carnot cycle model [27], as shown in Figure 3, is adopted to study the effects of the irreversibilities of heat conduction on the performance of the heat engine in the hybrid system, where the heat $\dot{Q}_H$ is the heat flux transferred from the high temperature heat reservoir, i.e., DCFC, at T to the working fluid at T_1, and $\dot{Q}_L$ from the working fluid at T_2 to the environment at T_0. In the model, it is assumed that the working fluid flows stably during the whole cycle period of the heat engine, that heat transfer between the reservoirs and the working fluid obeys Newton's law, and that the influence of other irreversible effects is negligible except the irreversibilities of heat conduction [27-29]. Thus, we obtain

$$\dot{Q}_H = U_1 A_1 (T - T_1), \tag{9}$$

$$\dot{Q}_L = U_2 A_2 (T_2 - T_0),\tag{10}$$

and

$$\frac{\dot{Q}_H}{T_1} = \frac{\dot{Q}_L}{T_2},\tag{11}$$

where U_1 and U_2 are, respectively, the heat conductivities between the working fluid and the heat reservoirs, A_1 and A_2 denote the heat transfer areas between the working fluid and the heat reservoirs.

As illustrated in Figure 3, a part of the waste heat produced in the DCFC is directly released as heat-leak to the environment, and this amount of the heat flow can be given by [18, 27, 29]

$$\dot{Q}_{loss} = KA_l (T - T_0),\tag{12}$$

where K is the convective heat-leak coefficient, and A_l denotes the effective heat-transfer area. Combined with the previous analysis, the rate of waste heat from the DCFC to the heat engine is given by

$$\dot{Q}_H = -\Delta \dot{H} - \dot{P}_{cell} - \dot{Q}_{loss}$$
$$= -\frac{JA}{n_e F} \Delta h - P_{cell} - KA_l (T - T_0).\tag{13}$$

Based on Eqs. (9)-(13), it can be easily proved that when $A_1 / A_2 = \sqrt{U_2 / U_1}$, the optimum efficiency and power output of the heat engine at given $\dot{Q}_H$ and A_h may be expressed as

$$\eta_{engine} = 1 - T_0 / \left(T - \dot{Q}_H / a_1 \right)$$
$$= 1 - \frac{1}{T / T_0 + a_2 J \left(1 - \eta_{cell} \right) + a_3 (T / T_0 - 1)},\tag{14}$$

and

$$P_{engine} = \dot{Q}_H \eta_{engine}$$
$$= a_1 \left[a_2 J T_0 \left(\eta_{cell} - 1 \right) - a_3 (T - T_0) \right] \eta_{engine},\tag{15}$$

where $a_1 = A_h U_1 U_2 / \left(\sqrt{U_1} + \sqrt{U_2} \right)^2$, $a_2 = \frac{A \Delta h}{T_0 a_1 n_e F}$, $a_3 = \frac{KA_l}{a_1}$, and $A_h = A_1 + A_2$ is the overall heat transfer area of the heat engine.

2.3. The regenerator

As illustrated in Figure 1, the regenerator works as a heat exchanger in the hybrid system, which heats the inlet reactants from the ambient temperature to the cell temperature by using the high-temperature outlet gas of the fuel cell. For the sake of simplicity, the regeneration process is assumed to be ideal. This assumption is well-founded as the efficiency of regenerators with the values of 98–99% have already been reported [11,15]. With the help of perfect regeneration, the fuel cell and hence

the whole hybrid system can be ensured to work normally and continually under the condition of steady-state.

2.4. The efficiency and power output of the hybrid system

Based on equations (2), (3), (14) and (15), one may obtain the efficiency and the power output of the entire DCFC-Carnot heat engine hybrid system, i.e.,

$$\eta_{hybrid} = \eta_{cell} + \left[1 - \eta_{cell} + \frac{a_3}{Ja_2}(\frac{T}{T_0} - 1) \right] \eta_{engine},$$ (16)

and

$$P_{hybrid} = \left(-JT_0 a_1 a_2 \right) \times \left\{ \eta_{cell} + \left[1 - \eta_{cell} + \frac{a_3}{Ja_2}(\frac{T}{T_0} - 1) \right] \eta_{engine} \right\}.$$ (17)

It is seen from equations (16) and (17) that the efficiency and the power output of hybrid system are larger than that of a sole DCFC, and the efficiency and power output are closely dependent on the irreversible losses including the irreversibilities within the fuel cell itself and originating from the heat transfer between the DCFC and the Carnot heat engine. In the next section, the general performance characteristics and the optimal criteria of the hybrid system will be revealed.

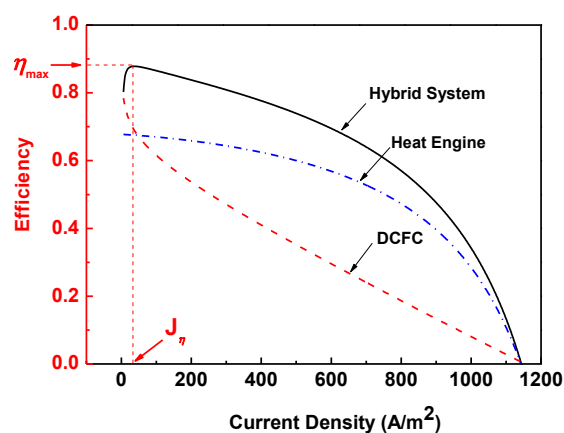## 3. GENERAL PERFORMANCE CHARACTERISTICS AND OPTIMAL CRITERIA

Optimal design and analysis of the hybrid system require a thorough understanding of its performance limitations. Equations (16) and (17) clearly show that the performance of the hybrid system depends on a set of thermodynamic and electrochemical parameters such as fuel cell temperature (T), operating current density (J), DCFC design parameter (N_s), and the parameters related to the heat transfer between the DCFC and the Carnot heat engine as well as the heat-leak to the surroundings, i.e., a_1, a_2 and a_3. In the following calculations, the parameters $a_1 = 1.0\,\text{W}\cdot\text{K}^{-1}$, $a_2 = -0.00185\text{m}^2\cdot\text{A}^{-1}$, $a_3 = 0.001$ are chosen. The related values of the input parameters not mentioned are summarized in Table 1, and these parameters are kept constants unless mentioned specifically.

By using Eqs. (16) and (17), the efficiency and power density of the hybrid system varying with the operating current density are presented in Figure 4, where $P^* = P/A$ is the power density. It can be clearly seen from Figure 4 that both the efficiency and power density of the hybrid system first increase and then decrease as the current density increases, and there exist a maximum efficiency η_{max} and a maximum power density P^*_{max}, where J_η and J_{P^*} are, respectively, the corresponding current densities at the maximum efficiency η_{max} and maximum power density P^*_{max}. Compared with the efficiency and power density of a sole DCFC, the efficiency and power density of the hybrid system is
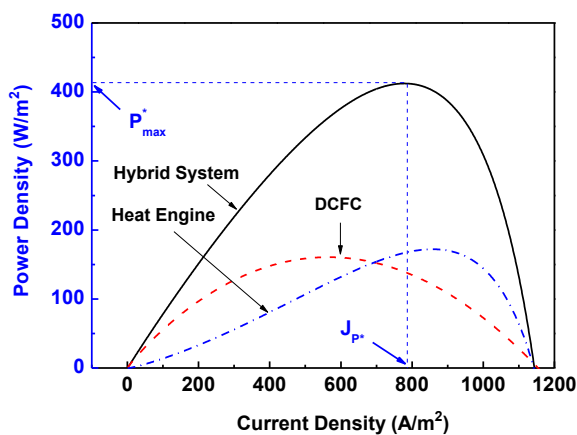
significantly improved because the waste heat in the fuel cell is further utilized through a Carnot heat engine. Both the efficiency and the power density augment with the increase of current density in the region of $J < J_\eta$, while both of them reduce with the increasing current density in the region of $J > J_{p^*}$. It is obvious that the regions of $J < J_\eta$ and $J > J_{p^*}$ are not optimal from the thermodynamic viewpoint although the hybrid system may work in these regions. Hence, the optimal region of the current density should be located in

$$J_\eta \le J \le J_{p^*}. \tag{18}$$

It shows that J_η and J_{p^*} determine the lower and upper bounds of the optimum current density, respectively. In the practical operation of the DCFC-Carnot heat engine hybrid system, engineers should choose a reasonable current density according to Eq. (18) to ensure that the system is operated in the optimal region.

(a)

(b)

Figure 4. The curves of (a) the efficiency, and (b) the power density varying with the current density, where $P^*_{hybrid} = P_{hybrid} / A$ is the power density, J_η and J_{P*} are the current densities at maximum efficiency η_{max} and maximum power density P^*_{max}, respectively.

Figure 5 shows the power density versus the efficiency at different operating temperatures, where P_m^* and η_m are, respectively, the power density at the maximum efficiency η_{max} and the efficiency at the maximum power output P_{max}^*. According to Figure 5, one can determine the optimally operating region, which has a negative slope in the part of the $\eta \sim P^*$ curve. When the hybrid system operates in this region, the power density will decrease as the efficiency increase, and vice versa. Thus, the optimal ranges of the efficiency and power density are given as

$$\eta_{max} \geq \eta \geq \eta_m ,\qquad\qquad(19)$$

and

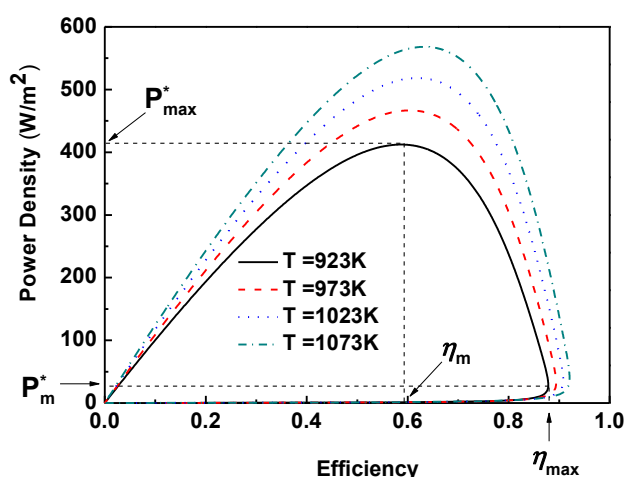$$P_m^* \leq P^* \leq P_{max}^* ,\qquad\qquad(20)$$

respectively.

Figure 5. The curves of the power density varying with the efficiency at different operating temperatures.

The above results show that P_m^*, η_m, P_{max}^* and η_{max} are four important parameters of the DCFC-Carnot heat engine hybrid system, where P_m^* and η_m determine the allowable optimum values of the lower bounds of the power density and efficiency, while P_{max}^* and η_{max} determine allowable optimum values of the upper bounds. It should note that the four important parameters closely depend on the thermodynamic and electrochemical parameters of the hybrid system and can be calculated numerically for the given values of other parameters.

4. RESULTS AND DISCUSSION

In general, since up to a half of the fuel energy of high-temperature fuel cells is waste heat, numerous investigators have carried out the research on high temperature fuel cell based hybrid

systems in order to increase the overall efficiencies of fuel cells [32-35]. However, the research activities about high temperature fuel cell based hybrid systems always focus on solid oxide fuel cells (SOFCs) and molten carbonate fuel cells (MCFCs), but the DCFC-heat engine hybrid system has never been studied. The established system model in this paper can be used to investigate the effects of various operating conditions and designing parameters on the performance of the DCFC hybrid system. In this section, a parametric analysis is carried out based on the performance criteria for the variation of operating parameters to characterize the system behavior. Next, the influences of different operating conditions on the performance of the system will be discussed respectively.
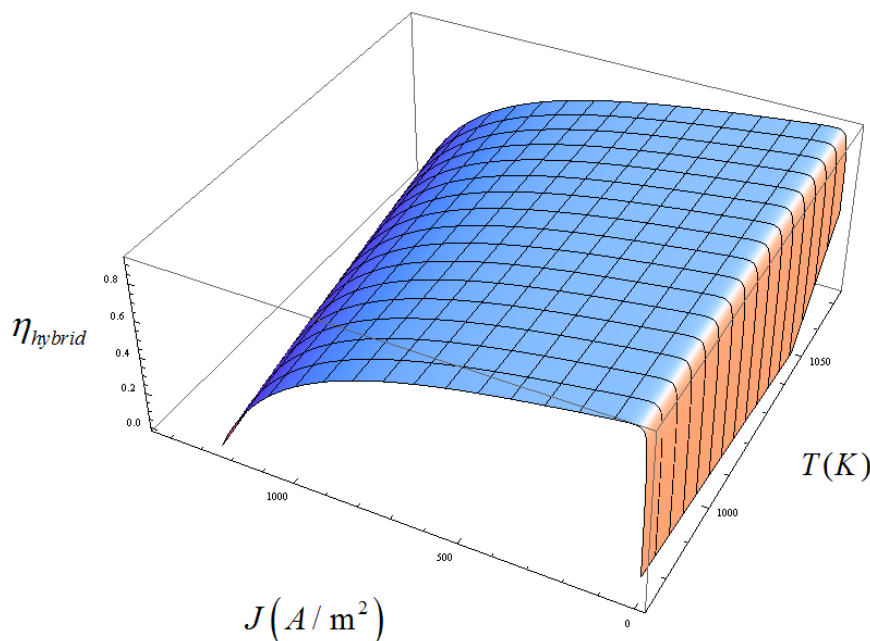

Figure 6. The three-dimensional curve of the efficiency varying with the current density and temperature, where the related values of parameters are listed in Table 1.

The operating temperature of the system is an important parameter because it directly affects the various overpotentials of the fuel cell as well as the performance of the heat engine. The power density and efficiency of the DCFC-Carnot heat engine hybrid system operating at a temperature range of $973 \sim 1073 \, K$ and a current density range of $0 \sim 1450 \, A \, m^{-2}$ are presented in Figure 6 and Figure 7. As shown in Figure 6 and Figure 7, the system performance will increase with the rise of the operating temperature. Meanwhile, the maximum efficiency, maximum power density, and the corresponding current densities will also be slightly increased as the operating temperature is increased. Generally, the higher operating temperature is more favorable for a DCFC-Carnot heat engine hybrid system within the allowable range of various component materials. In addition, for the problem how to select the operating temperature of the system, one may simultaneously consider the investment cost and the degradation issue involved in manufacturing both a stack with the required thermal stability as well as

the whole system that can be operated at that specified temperature. A similar result has appeared in other papers for high-temperature fuel cell hybrid system [11-15], thus it may be seen as a same result for this kind of systems.

For DCFC-Carnot heat engine hybrid system, the structure of DCFC also has great influence on the performance of the system. We will take the anode dimension as an example to discuss the effect of internal structure. As shown in Figure 8, the curves of the efficiency and the power density varying with the current density at different N_s, i.e., different anode dimension, are given. From Figure 8, it is evident that the influence of anode dimension on the maximum power density is larger than that on the maximum efficiency. In addition, the greater the anode dimension, the smaller efficiency and power density will be. It is distinct that the ohmic overpotential of DCFC will increase as the growth of the number of slabs, and accordingly, the performances of DCFC and the hybrid system will be deteriorated.
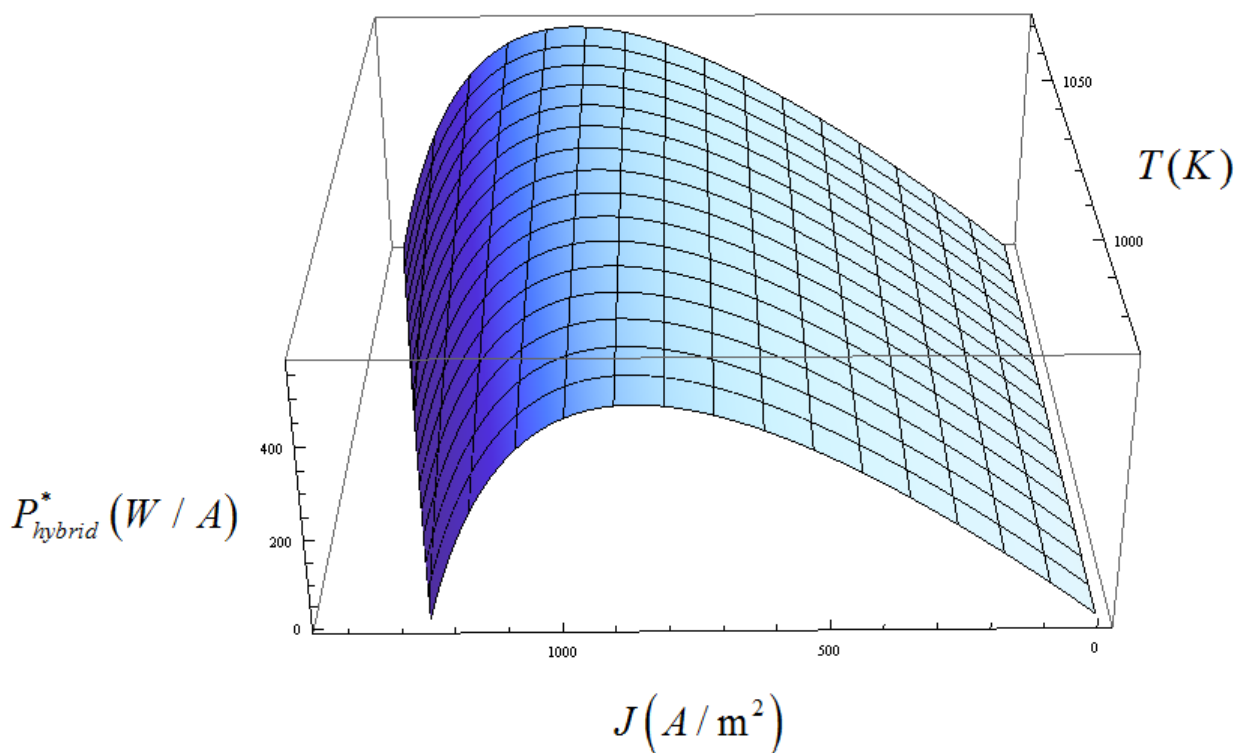

Figure 7. The three-dimensional curve of the power density varying with the current density and temperature, where the values of the relevant parameters are the same as those used in Figure 6.

Last but not least, it is noteworthy to investigate the parameters related to the heat transfer between the DCFC and the Carnot heat engine as well as the heat-leak to the surroundings, i.e., a_1, a_2 and a_3. By using Eqs. (16) and (17), it can be easily proved that the power density and efficiency of the hybrid system are monotonically increasing functions of a_1. a_1 is a parameter to measure the irreversibility of finite rate heat transfer in the heat engine, the larger the parameter a_1, the smaller the

heat transfer irreversibility in the heat engine is and the better the performance of the hybrid system can be expected.
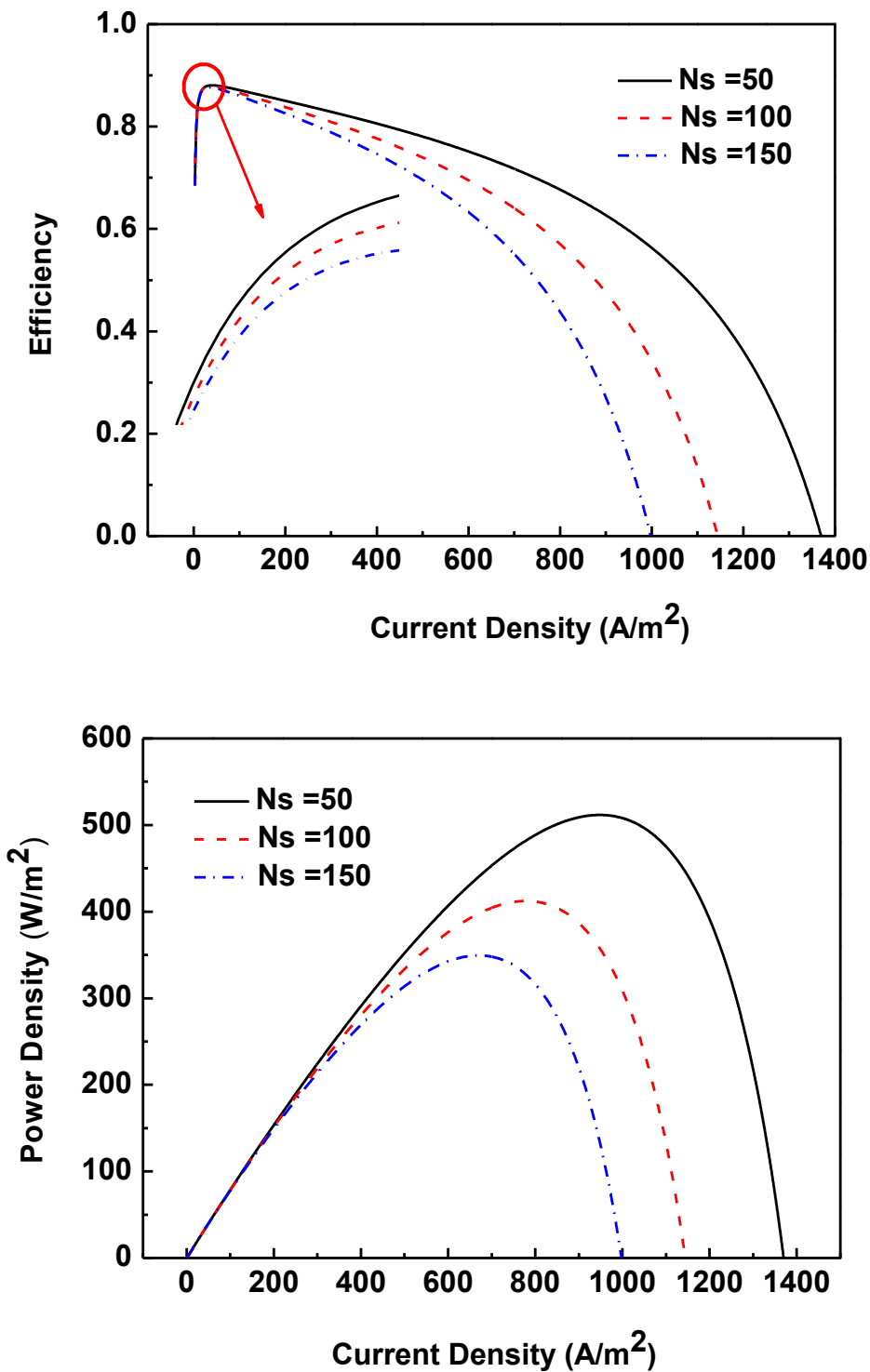

Figure 8. The curves of (a) the efficiency, and (b) the power density varying with the current density at different N_s.
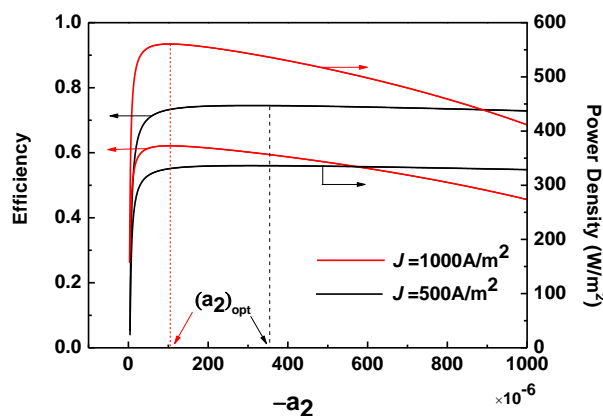
Figure 9. The curves of the efficiency and power density of the hybrid system varying with the parameter a_2.

The parameter a_2 is a colligation measurement for the systemic structure. It may be proved that there is a common extreme condition of $\partial \eta_{hybrid} / \partial a_2 = \partial P_{hybrid} / \partial a_2 = 0$ for the hybrid system. It implies the fact that there is a common optimum value of $(a_2)_{opt}$ at which both the power output and efficiency will attain their maxima simultaneously, as shown in Figure 9.

From Eqs. (16) and (17), it can be also proved that the power density and efficiency of the hybrid system are monotonically decreasing functions of a_3. Its physical meaning can be easily explained as follows: a_3 is a synthesized parameter to measure the heat-leak irreversibility from the fuel cell to the surroundings. The smaller the parameter a_3 is, the better the performance of the hybrid system will be.

5. CONCLUSIONS

The importance of present paper lies in a new hybrid system is established to use the waste heat generated in the high-temperature DCFC. It is found that the performance of the DCFC can be greatly enhanced by using a Carnot heat engine for further power generation. Moreover, the effects of some important parameters such as temperatures, operating current density, the internal configuration of DCFC, and a variety of irreversible losses on the performance of the DCFC are illustrated. The optimum criteria of some important performance parameters such as the power density and efficiency of the hybrid system are given. The results obtained here may provide some theoretical basis for the performance enhancement of practical DCFCs.

References

1. A Di Carlo, E Bocci, V Naso, *Int J Hydrogen Energy*, 38 (2013) 532.
2. M Santin, A Traverso, L Magistri, A Massardo, *Energy*, 35 (2013) 1077.
3. H Park, *Energy Convers Manage*, 81 (2014) 220.
4. C Li, Y Shi, N Cai, *J Power Sources*, 195 (2010) 4660.
5. D Cao, Y Sun, G Wang, *J Power Sources*, 167 (2007)250.
6. N Cherepy, R Krueger, K Fiet, A Jankowski, J Cooper, *J Electrochem Soc*, 152 (2005) 80.
7. Q Liu, Y Tian, C Xia, L Thompson, B Liang, Y Li, *J Power Sources*, 185 (2008) 1022.
8. J Bockris, J Kim, *J Appl Electrochem*, 27 (1997) 890.
9. K Hemmes, M Houwing, N Woudstra, *J Fuel Cell Sci Technol*, 7 (2010) 051008.
10. A Elleuch, A Boussetta, K Halouani, *J Electroanalyt Chem*, 668 (2012) 99.
11. Y Zhao, J Chen, *J. Power Sources* 186 (2009) 96.
12. H Zhang, G Lin, J Chen, *Int J Electrochem Sci*, 6 (2011) 4714.
13. H Zhang, S Su, G Lin, J Chen, *Int J Electrochem Sci*, 7 (2012) 3420.
14. L Chen, H Zhang, S Gao, H Yan, *Energy*, 64 (2014) 923.
15. L Chen, S Gao, H Zhang, *Int. J. Electrochem. Sci*., 8 (2013)10772.
16. J Ruflin, A Perwich, C Brett, J Berner, S Lux, *J Power Sources*, 213 (2012) 275.
17. H Kim, J Bae, D Choi, *Int. J. Hydrogen Energy*, 38 (2013) 4782.
18. C Li, Y Shi, N Cai, *J Power Sources*, 196 (2011)754.
19. Y Zhao, C Ou, J Chen, *Int. J. hydrogen energy*, 33 (2008) 4161.
20. H Zhang, L Chen, J Zhang, *J Chen, Energy* 68 (2014) 292.
21. J Cooper. Direct conversion of coal and coal-derived carbon in fuel cells. ASME paper No. KH-3, 2004.
22. K Hemmes, M Houwing, *N Woudstra*, 7 (2010) 051008.
23. D Vutetakis, DR Skidmore, HJ Byker, *J Electrochem Soc* 134 (1987) 3027.
24. Y Xie, Y Tang, J Liu, *J Solid State Electrochem*, 17 (2013)121.
25. X Li, H Zhu, R De Marco, A Dicks, Bradley J, Liu S, Lu GQ, *Ind Eng Chem Res*, 47 (2008) 9670.
26. G Wilemski, *J Electrochem Soc* 130 (1983) 117.
27. J Chen, *J. Appl. Phys*., 72 (1992) 3778.
28. J Chen, Z Yan, *J. Appl. Phys*, 63 (1988) 4795.
29. A Durmayaz, O Sogutb, B Sahinc, H Yavuz, *Prog. Energy Combust. Sci*., 30 (2004) 175.
30. MR Quddus, Y Zhang, AK Ray, *Chem. Eng.*, 165 (2010) 639.
31. N Autissier, F Palazzi, F Marechal, J van Herle, D Favrat, *J. Fuel Cell Sci. Technol*., 4 (2007) 123.
32. J W Burbank, D Witmer, F Holcomb, *J Power Sources*, 193 (2009) 65.
33. C Haynes, *J Power Sources*, 92 (2001) 199.
34. D Sa´nchez, R Chacartegui, M Torres, T Sa´nchez, *J Power Sources*, 192 (2009) 84.
35. J Qin, W Zhou, W Bao, D Yu, *Int J Hydrogen Energy*, 35 (2010) 356.